Effects of Thickness and Annealing on the Structural and Optical Properties of Chemical Bath Deposited CdS Thin Films

Rodrigo Cue S.[1], S. Velumani[2,*], P.J. Sebastian[3], J.A. Chávez-Carvayar[4]

[1]Tecnologico de Monterrey, E.Garza Sada #2501, C.P. 64849, Monterrey, N.L., México
[2]Ingeniería Eléctrica (SEES), CINVESTAV, Zacatenco, C. P. 07360, México D. F., México
[3]CIE-UNAM, Privada Xochicalco S/N, C. P. 62580, Temixco, Morelos, México
[4]Instituto de Investigaciones en Materiales, UNAM, México D.F., México

Abstract: *Present work focuses on the preparation and characterization of II–VI thin film semiconductor compound Cadmium Sulfide (CdS), commonly used as window layer in polycrystalline thin-film photovoltaic cells. CdS thin films were prepared by chemical bath deposition (CBD) in six different thicknesses and subjected to heat treatment at five different temperatures in nitrogen atmosphere, in order to find the appropriate film for perfect window layer in copper indium diselenide (CIS)/CdS photovoltaic cells. Structural and optical characterizations were carried out by X-ray diffraction and UV-VIS-NIR spectrometer respectively. Both the Hawleyite (cubic) and Greenockite (hexagonal) phases were observed, the latter being most predominant. Films show good transmittance in visible region and the band gap was found to decrease with the increase in thickness and annealing temperature.*

1. INTRODUCTION

Cadmium Sulfide (CdS) is a II-VI semiconductor compound with the energy band gap of 2.43 eV for the bulk material, which lies near the maximum photon energy of the solar radiation spectrum. CdS thin films find their potential application in the area of high efficiency photovoltaic cells. They are used especially as a partner material as well as suitable window layer for $CuInSe_2$ and CdTe based photovoltaic cells. Common methods for depositing CdS thin films are vacuum evaporation [1, 2], sputtering [3, 4], spray pyrolysis [5, 6], molecular beam epitaxy [7, 8], electrode-position [9, 10] and chemical bath deposition (CBD) [11, 12]. CBD is an "electroless" technique that is attractive as a simple and low cost method for achieving good-quality CdS films. Additionally CBD is an appropriate technique for coating surfaces of any morphology and geometry and therefore this technique is particularly suitable for industrial applications. It is well known that deposition conditions (bath composition, reagent concentrations, temperature, pH, etc.) strongly influence the film stoichiometry, microstructure and crystallinity, which directly determine the opti-

cal and electrical properties of CdS films [13]. The transition of polycrystalline CdS films from metastable cubic structure to stable hexagonal structure can be produced by thermal annealing in a controlled atmosphere [14, 15-19]. The structural transition of the cubic CdS films is accompanied by changes in the energy band gap of the annealed films. Even though lot of research has been carried out on CBD CdS films, under certain conditions, CBD grown CdS films show better optical and electrical characteristics resulting in better cell performance in solar cells. Therefore in the present work CBD CdS thin film were prepared to understand relation effect of thickness and annealing over its structural and optical properties.

2. EXPERIMENTAL DETAILS

The films were deposited on commercial glass slides of 76 mm x 25 mm cleaned in propanol, ethanol and methanol ultrasonically, then etched in a 5% HF solution and finally washed again ultrasonically with methanol. CdS thin films were prepared by the decomposition of thiourea as the sulfur source in an alkaline solution of cadmium salts according to the following reaction [11, 15]:

$$Cd(NH_3)_4^{2+} + SC(NH_2)_2 + 2OH^- \rightarrow CdS + CH_2N_2 + 4NH_3 + 2H_2O \quad (1)$$
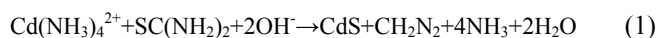
*To whom correspondence should be addressed: Email: velu@cinvestav.mx or vels64@yahoo.com

The total volume (100 ml) of the chemical bath is formed by an aqueous solution from the following concentrations of each reactant: 0.1M cadmium nitrate ($Cd(NO_3)_2$), 1M sodium citrate ($Na_3C_6H_5O_7$), 30% ammonia (NH_4OH) and 1M thiourea ($CS(NH_2)_2$). The cleaned substrates were mounted vertically using a Teflon holder in a closed vessel. The temperature of the deposition process was 70 °C. All the solutions that were used in deposition were clear solutions without precipitation. The bath solution was held still without stirring. CBD of the CdS can be found in more detail in other articles [11]. Each deposited film was retired one by one from the bath after 45, 75, 105, 135, 165 and 195 minutes. After the deposition, the CdS films were ultrasonically washed with methanol to remove the loosely adhered CdS particles on the film and finally dried in air. The resulted transparent films presented a pale yellow color with bright surface and good adherence to the substrates. The as-deposited films were annealed for one hour in nitrogen atmosphere at different temperatures ie., 200, 250, 300, 350 and 400 ºC. The thicknesses of all the samples were measured using a thickness profile-meter. Structural, morphological and optical properties of as deposited and annealed films have been studied.

2.1. Structural analysis

Structure of the films were analyzed using a Grazing Incidence X-ray diffractometer (Rigaku D-Max 2000, using Cu-Kα radiation with λ=1.5406 Å). Measurements were made for 2θ values between 20-70° in steps of 0.03° with a count time of 5 sec and a grazing angle equal to 1.5º. Grain size (D) was calculated using the Scherrer formula [20]

$$D = \frac{k\lambda_X}{\beta Cos\theta} \tag{2}$$

where D is the grain size, k is the Scherrer constant (0.94), λ_x is the wavelength of the X-ray used, β is the full width at half maximum (FWHM) and θ is the Bragg angle.

The strain (ε) was calculated from the slope of the $\beta cos\theta$ versus $sin\theta$ plot using the relation.

$$\beta = \frac{\lambda}{D\cos\theta} - \varepsilon\tan\theta \tag{3}$$

The dislocation density and the number of crystallites per unit surface area have been determined by the following formulas [21]

$$\delta = \frac{1}{D^2} \tag{4}$$

$$N = \frac{t}{D^3} \tag{5}$$

Where δ is the dislocation density, N the number of crystallites per unit surface and t the thickness of the thin film.

The lattice parameter a for the cubic structure was evaluated from the equation [22]

$$a = d\sqrt{(h^2 + k^2 + l^2)} \tag{6}$$

And for the hexagonal structure, the lattice parameters a and c were evaluated from the equation [23]

$$\frac{1}{d^2} = \frac{4}{3}\frac{h^2 + hk^2 + k^2}{a^2} + \frac{l^2}{c^2} \tag{7}$$

Transmission Electron Microscopy Jeol TEM 1200 EX microscope operating at 120 kV and 70 A was also used for crystallites measurement and Selected Area Electron Diffraction (SAED) patterns have been obtained.

2.2. Surface morphology and compositional analysis

The morphology of the deposited CdS has been determined by Scanning Electron Microscopy (SEM) using a Stereoscan 440 microscope. Atomic Force Microscopy (AFM) analysis of the CdS thin films was performed using Veeco Instruments Multimode SPM in the tapping mode with a 10 im piezoelectric scanner at Scan Speed of 0.7 Hz. Three AFM images of different magnification of the surface were obtained, at atmospheric pressure and room temperature.

2.3. Optical analysis

The transmittance spectra of CdS thin films were measured in equipment consisting of Shimadzu 3101 PC UV-VIS-NIR spectrometer in the wavelength range 250-2500 nm. The spectral distributions of transmittance of the films with different thicknesses were determined at room temperature. The substrate absorption is corrected by introducing an uncoated clean glass in the reference beam. The absorption coefficient α can be calculated using the relation [24]

$$\alpha = \frac{2.303\log\left(\frac{1}{T}\right)}{t} \tag{8}$$

Where T is the transmittance and t is the film thickness.

The extinction coefficient and the refractive index can be evaluated from the relations

$$\alpha = \frac{4\pi kt}{\lambda} \tag{9}$$

$$T = \frac{n_2}{n_0}\frac{(1+\delta_1)^2 + (1+\delta_2)^2}{1+(\delta_1^2\delta_2^2) + 2\delta_1\delta_2\cos 2\Gamma} \tag{10}$$

where

$$\delta_1 = \frac{n_0^2 + n_1^2}{(n_0 + n_1)^2}, \quad \delta_2 = \frac{n_1^2 - n_2^2}{(n_1 + n_2)^2}, \quad \Gamma = \frac{2\pi n_1 t}{\lambda} \tag{11}$$

Where λ is the wavelength of the incident radiation, n_0, n_1, n_2 are the refractive indices of air, film and glass, respectively. Substituting the experimental values for T, t, n_0 and n_2, the above equation can be solved for n_1 and k using the method of iteration until the desired convergence is achieved.

2.4. Annealing of the films

Effects of Thickness and Annealing on the Structural and Optical Properties of Chemical Bath Deposited CdS Thin Films / J. New Mat. Electrochem. Systems

9

Table 1. Structural parameters of the hexagonal structures of CdS films with thicknesses 530, 1050 and 1900 Å.

Thickness (Å)	Structure	Lattice (Å)		Grain Size (Å)	Dislocation density (δ) (10^{14} lines/m^2)	Numb. of crystallites/unit area (10^{15}m^{-2})	Strain (ε)
		a	c				
530	Hexagonal	4.1526	6.5627	135	64	58	2.25
1050	Hexagonal	4.1478	6.7380	144	53	57	2.33
1900	Hexagonal	4.0816	6.6096	153	48	67	1.83

The as-deposited films were annealed in nitrogen atmosphere at the temperatures of 200, 250, 300, 350 and 400°C. The annealing time was 1 hour. After annealing, they were kept in the furnace with the nitrogen atmosphere for another hour until they reached room temperature. All the characterizations have been made for the same samples before and after annealing.

3. RESULTS AND DISCUSSION

3.1. Effect of Thickness
3.1. Structural Studies

The X-ray diffraction patterns of the CdS films of thicknesses
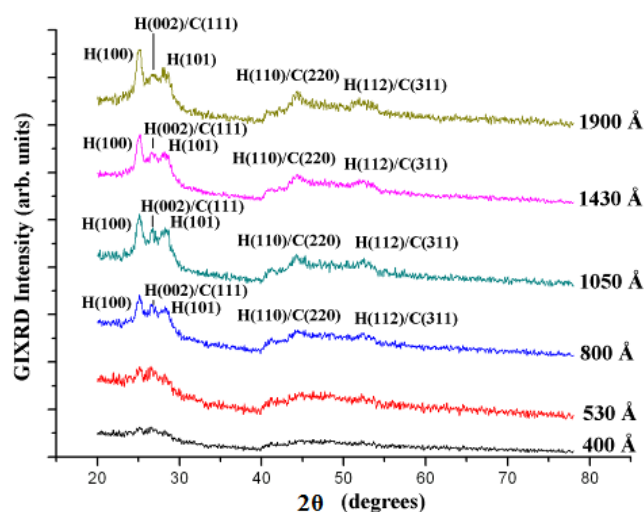
Figure 1. XRD pattern of the CdS films with thicknesses 400, 530, 800, 1050, 1430 and 1900 Å.

400, 530, 800, 1050, 1430 and 1900 Å are shown in Fig. 1. Several diffraction peaks can be observed, indicating that the films are polycrystalline in nature. Also the peak intensity increases as the film thickness increases and this is due to the growth of the deposited material involved in the CBD process [15, 25]. For the thinner films of 400 and 530 Å there are no considerable peaks, thus there is no representative structure. But with the increase in thickness, the peaks corresponding to both the hexagonal and cubic structures become visible, indicating that there is a mixture of phases [26]. The peak at 2θ=25.12° corresponds to the hexagonal (100) plane, the peak at 26.68° is associated with the mixture of hexagonal (002) and cubic (111) planes, the peak at 28.55° corresponds to the hexagonal (101) plane, the peak at 44.26° is associated with the hexagonal (110) and cubic (220) planes, and the peak at 52.39° is associated with the hexagonal (112) and cubic (311) planes. The intense peak that appears at 25.12° indicates the preferential orientation of the hexagonal plane (100).

The identification and assignments of the observed diffraction patterns were made using the JCPDS data and by comparison with previous published results [27, 28].

The structural parameters are shown in Table 1. From these values, it can be seen that the films present a polycrystalline structure. It can be seen that the grain size increases while increasing the thickness.

The structure of CdS films was also observed using TEM as shown in Fig. 2(a) and 2(c). It is supposed that each particle is composed of fine crystallites (white), whose sizes were determined by XRD technique. The inset of the corresponding figure showed the Selected Area Electron Diffraction (SAED) patterns presented in Fig 2(b) and 2(d). Each pattern show a set of concentric rings due to the random orientation of the crystallites, corresponding to diffraction from different planes of the crystallites [27]. The dif-
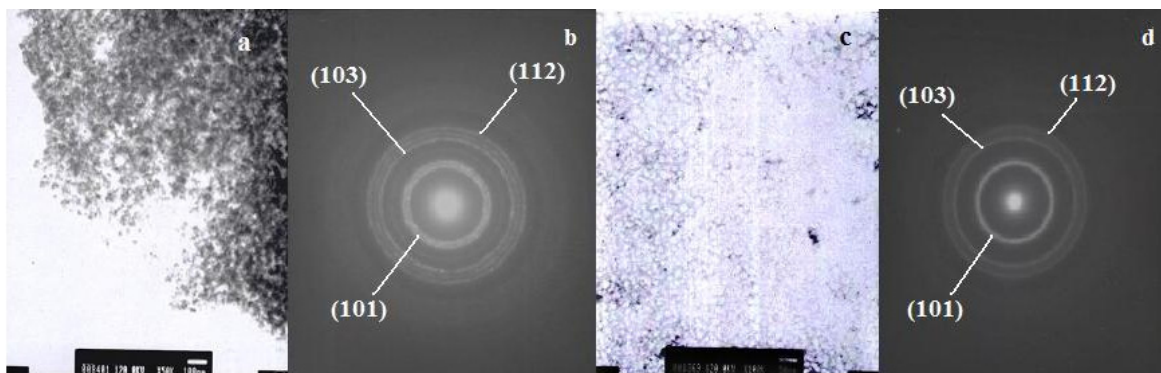
Figure 2. (a) and (c) show transmission electron micrographs of CdS thin films of thickness 400 Å and 1900 Å, respectively. (b) and (d) show SAED patterns of CdS thin films of thickness 400 Å and 1900 Å respectively.
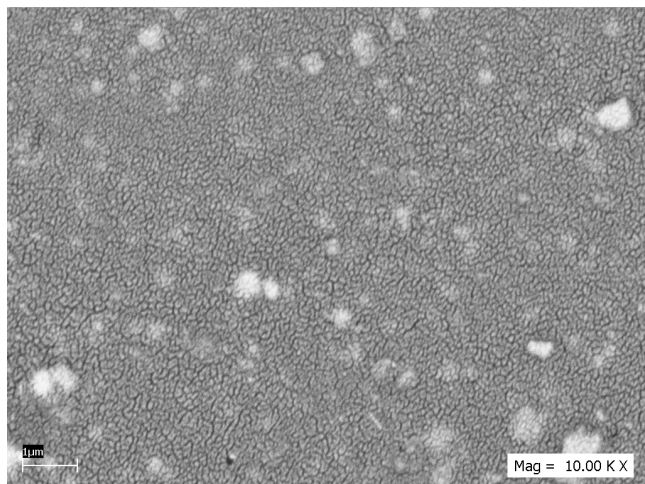
Figure 3. SEM micrographs of 1900 Å film with amplification of 10,000×.
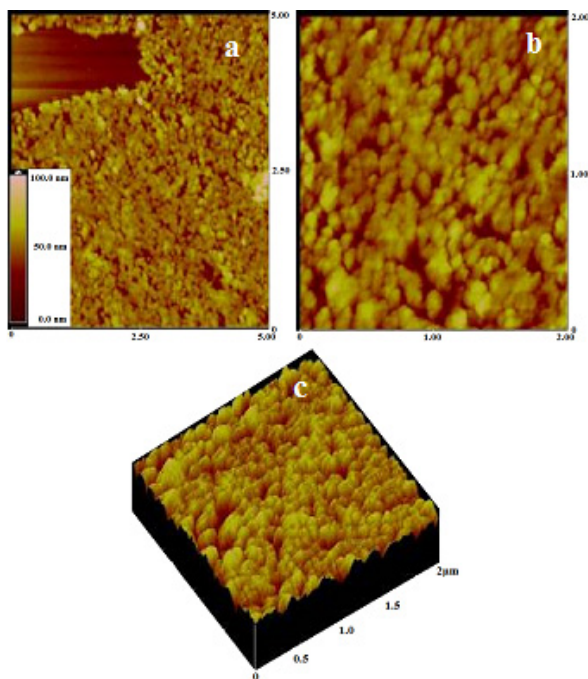
Figure 4. Two dimensional AFM images of the 400 Å film with areas of (a) 5 × 5 μm², (b) 2 × 2 μm² and (c) a three dimensional AFM image of the 400 Å film with an area of 2 × 2 μm².

fraction rings have been indexed and correspond to (101), (103), and (112) planes of the hexagonal CdS phase (JCPDS card, File No.41-1049). The thick rings in Fig. 2(b) show that the crystals are not well defined at the thickness of 400 Å, but at 1900 Å Fig. 2(d) the crystals structure is clear and therefore the rings are thinner.

3.2. Surface morphology and composition
   Surface morphology of the CBD-CdS thin films is depicted in Fig. 3. Colloidal particles precipitate over the film during deposition and can be clearly seen as white crystals.
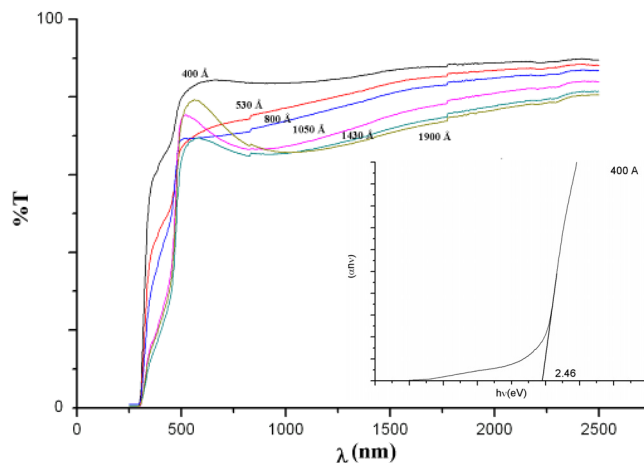
Figure 5. Spectral distribution of transmittance of the films with different thicknesses. Inset shows the band gap calculation of the 400 Å film.

Table 2. Band gap, absorption coefficient, refractive index and extinction coefficient (α, n, k at 600nm) of CdS thin films with different thicknesses.

Thickness (Å)	Band gap (eV)	α Absorption coefficient (10^6)	n Refractive index	k Extinction coefficient (10^{-2})
400	2.57	3.87	2.70	3.25
530	2.54	4.23	2.81	3.71
800	2.53	4.66	2.85	2.88
1050	2.50	6.44	2.89	2.91
1430	2.46	7.19	2.85	2.03
1900	2.40	7.89	2.68	1.54

   AFM was used to investigate the morphology of CdS film. Fig. 4 shows two dimensional (2-D) AFM images obtained from (a) 5 × 5 μm² and (b) 2 × 2 μm² areas of the film sample with a thickness value of 400 Å. For each condition, the left image shows the height profile of the sample surface whereas the picture on the right shows the phase profile of the signal measured in each point on the surface.
   In Fig. 4(a), the z-scale is shown at the left and good agreement between the profile meter and the AFM technique is observed. The image in Fig. 4(b) shows good uniformity of the particles and an average particle size of 62 nm.
   Fig. 4(c) presents a three dimensional AFM image of the same 400 Å film. It is observed that the film shows no agglomeration and a normal thin film growth.

3.3. Optical Properties
   The spectral distribution of the transmittance of the films with different thicknesses is shown in Fig. 5.

3.3.1. The dependence of optical properties of CdS

Effects of Thickness and Annealing on the Structural and Optical Properties of Chemical Bath Deposited CdS Thin Films
/ J. New Mat. Electrochem. Systems

11
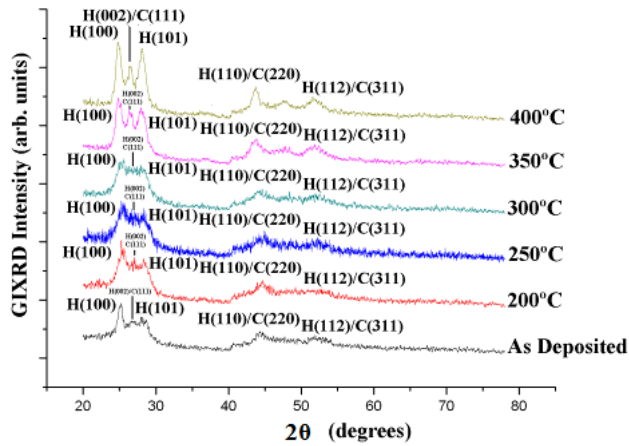
Figure 6. XRD pattern of the annealed CdS films.

films on the thickness

A set of CBD CdS films with thicknesses values of 400, 530, 800, 1050, 1430 and 1900 Å was produced. The band gap values were obtained by plotting *(αhν)²* versus *E(eV)* and taking the slope of the graph at the beginning of band-to-band absorption as can be seen in the inset of Fig. 5.

The band gap, refractive index and extinction coefficient values corresponding to different thicknesses of the CBD-CdS thin films are given in Table 2.

It can be noted from Table 2 that the maximum band gap is obtained at 400 Å, It is observed that the band gap decreases with increase of film thickness. Similar observation of decrease in band gap with thickness was reported by Pantoja and Mathew [11]. The decrease in the band gap can be due to the influence of various factors such as grain size, structural parameters, carrier concentration, presence of impurities, deviation from stiochiometry of the film and lattice strain [11,13,15]. A detailed analysis is needed to bring out the effect of each of these parameters on the value of band-gap energy. However, we have observed that the lattice parameters, grain size and the strain have a direct dependence on the film thickness. Hence, we consider that the observed decrease in band gap with increasing thickness is due to the increase in lattice strain. It can be seen that the optical absorption coefficient of the films increases by increasing the thickness.

3.4. Effect of Annealing
3.4.1. Structural Studies

The diffraction patterns of the film of thickness 1900 Å annealed at 200, 250, 300, 350 and 400 °C are shown in Fig. 6. It is observed that the peaks at 25.12° and 28.55° get broadened as the annealing temperature increases and become more pronounced at 400 °C which can be attributed to the recrystallization from cubic to hexagonal. The peak at 26.68° is not detectable in the as-deposited film, although it can be observed after annealing at 200-300 °C and becomes more intense when annealed at 350-400 °C, as it is clearly evident that it will be due to the growth of crystals. The peak at 44.26° is not detectable in the as-deposited film, yet its intensity

Table 3. Structural parameters of hexagonal structures of the CdS films at room temperature and annealed at 200, 250, 300, 350 and 400 °C.

Annealing Temperature (°C)	Structure	Lattice (Å)		Grain Size (Å)	Dislocation density (δ) (10^{14} lines/m²)	Numb. of crystallites/unit area (10^{15}m⁻²)	Strain (ε)
		a	*c*				
RT	Hexagonal	4.0816	6.6096	153	48	67	1.83
200	Hexagonal	4.069	6.9514	162	38	45	1.72
250	Hexagonal	4.0332	7.222	184	29	29	1.84
300	Hexagonal	4.0963	7.2431	182	30	32	1.86
350	Hexagonal	4.0929	6.9154	184	29	30	1.83
400	Hexagonal	4.139	6.8576	184	30	32	1.88
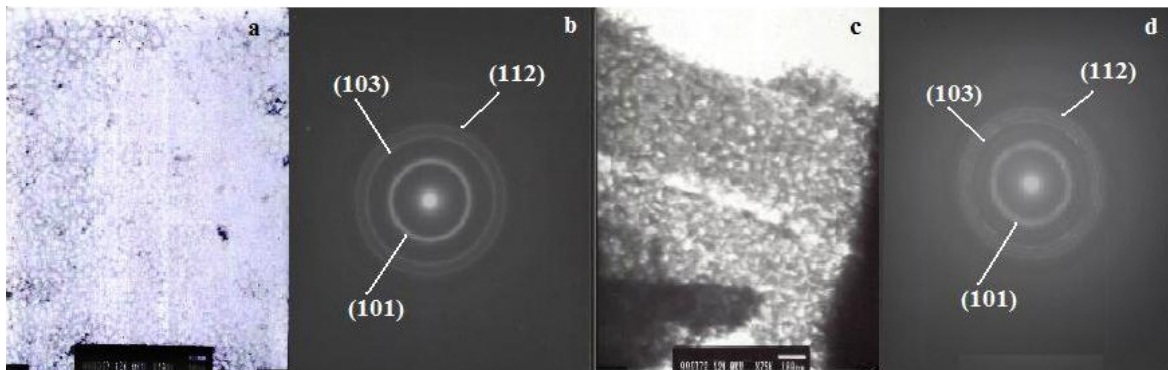
Figure 7. (a) and (c) show transmission electron micrographs for as-deposited and annealed CdS thin films at 400 °C, respectively. (b) and (d) show SAED patterns for as-deposited and annealed CdS thin films at 400 °C, respectively.
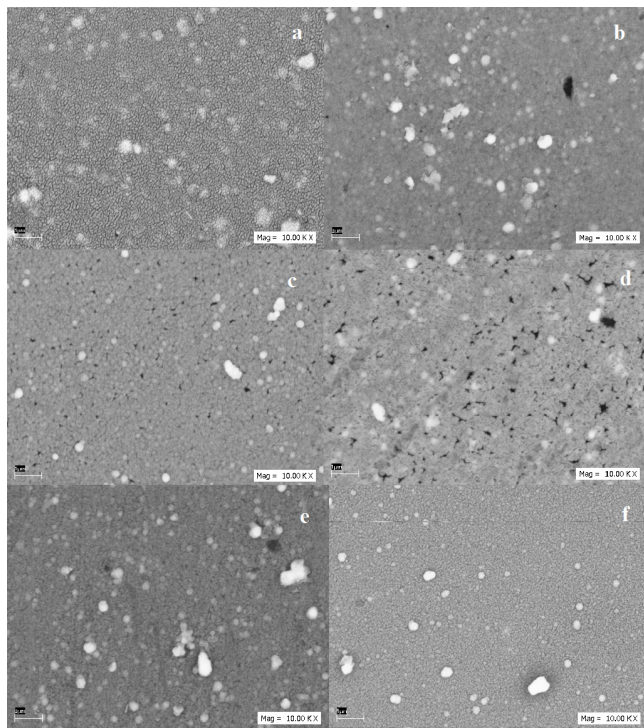
Figure 8. SEM micrographs of CdS thin films (a) as-deposited, (b) annealed at 200 °C, (c) at 250 °C, (d) at 300 °C, (e) at 350 °C and (f) at 400 °C.

increases as the annealing temperature increases which is due to more orderliness in the crystal structure in the films. By examining the whole peaks it can be concluded that these films contain a mixture of both hexagonal and cubic structures. Since the peak at 25.12°, which corresponds to the hexagonal (100) plane, becomes sharper and higher as the annealing temperature increases, it can be assumed that the percentage of hexagonal structured crystallites in the film increases when films are annealed at higher temperatures.

The structural parameters are shown in Table 3. It can be seen that for the hexagonal structure, the grain size increases with increase in the annealing temperature. The optical properties, such as the band gap energy, are quite dependent on the crystal sizes [28].

The annealing effect on both the morphology and the structure can be observed in the TEM images presented in Fig. 7. The as-deposited films are presented as small crystallites with a higher percentage of amorphous materials. The SAED pattern of this film shows continuous and thick rings, while for the film annealed at 400 °C there are some bright spots surrounding the rings which correspond to bigger crystallites [30].

3.4.2. Surface morphology and composition

Fig. 8 includes SEM micrographs of CdS films as-deposited and annealed at 200, 250, 300, 350 and 400 °C. These images show how the grains evolve as the annealing temperature is increased. Besides the colloidal particles, it can be observed that the grains adopted a "rice and pyramidal" shape at an annealing temperature of 400 °C, which it is very desirable for a window layer as this configuration allows higher absorption of the incident light.

The morphology of the annealed CdS films was also investigated by AFM. Fig. 9 shows 3D AFM images of the surface of the films after exposing them to the heat treatment. At 200 °C the films pre-
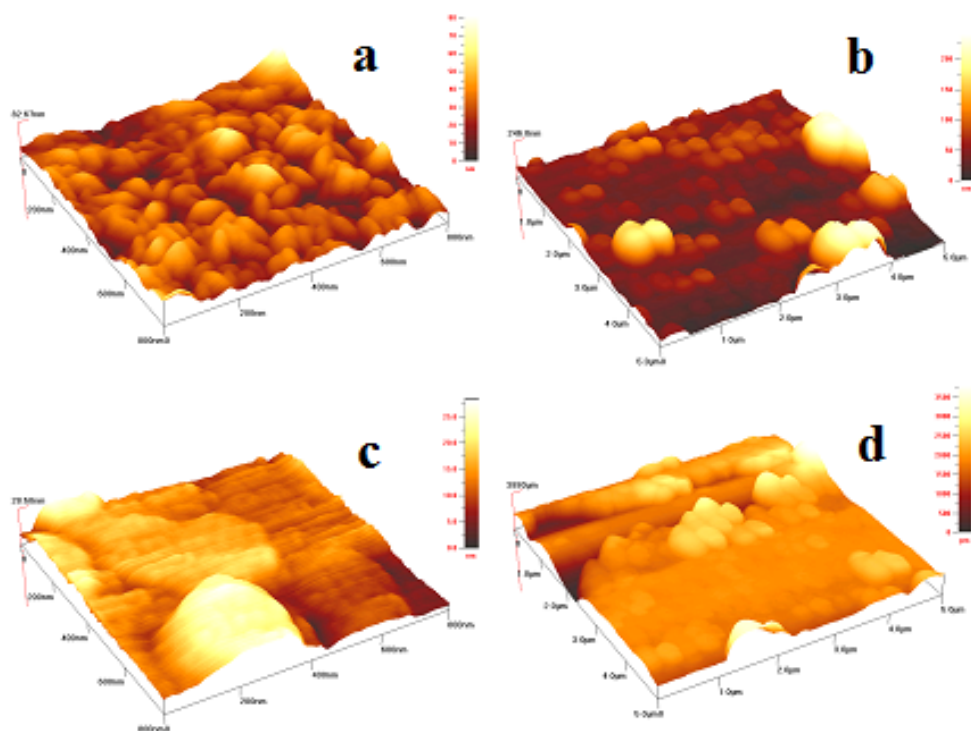
Figure 9. Three dimensional AFM images of CdS thin films annealed at (a) 200, (b) 250, (c) 350 and (d) 400 °C.

Effects of Thickness and Annealing on the Structural and Optical Properties of Chemical Bath Deposited CdS Thin Films / J. New Mat. Electrochem. Systems

13
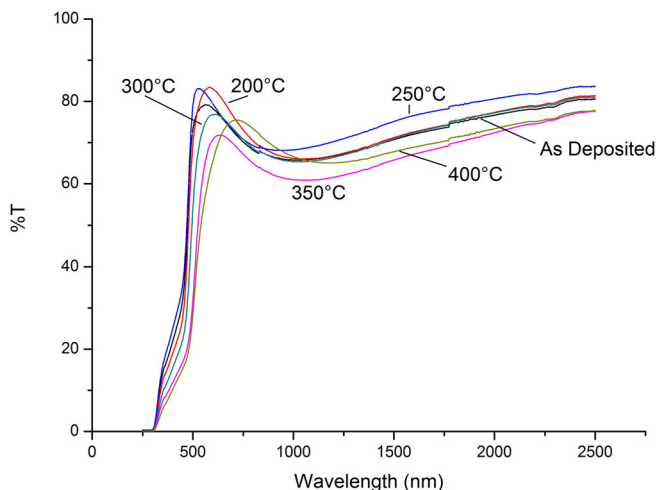
Figure 10. Spectral distribution of transmittance of the films with different annealing temperatures.

Table 4. Band gap, absorption coefficient, refractive index and extinction coefficient (α, n, k at 600nm) of CdS thin films annealed at different temperatures.

Temperature (°C)	Band gap (eV)	α Absorption coefficient (10^6)	n Refractive index	k Extinction coefficient (10^{-2})
RT	2.54	7.89	2.88	1.54
200	2.52	4.36	2.87	1.49
250	2.52	3.17	2.89	1.44
300	2.45	1.39	2.88	1.55
350	2.36	1.82	2.87	1.79
400	2.34	2.21	2.75	1.39

sent clusters with a globular surface morphology, and as the temperature increases, the surface becomes smoother and bigger crystallites are formed.

3.4.3. Optical Properties

The spectral distribution of transmittance of the films at different annealing temperatures is shown in Fig. 10**.**

The band gap, refractive index and extinction coefficient values corresponding to different annealing temperatures of the CBD-CdS thin films are given in Table 4. The optical energy gap and the refractive index decrease while increasing the annealing temperature [14, 29]. The temperature dependent parameters that affect the band gap are reorganization of the film, sulfur evaporation and self-oxidation of the film. The reorganization of the film should occur at all annealing temperatures. By filling the voids in the film one expects denser films and lower energy gaps. The color of the films changes from yellow to brownishyellow. Even though the annealing process was carried out in nitrogen atmosphere, oxidation of film surfaces always occurs as reported by Metin et al [14]. The oxidation may be the following reaction:

$$Cd(OH)_2 \rightarrow CdO + H_2O \qquad (11)$$

Here one may expect some of the $Cd(OH)_2$ precipitates in the film and the surface change to CdO after heating and gives out water vapor that causes further oxidation. Even for small percentage of oxidation we can observe a sharp decrease in the energy gap value. The reason is that in a mixture of CdS+CdO, the energy gap of CdO also contributes and finally it is measure of both elements during the transmission analysis. In addition the oxidation may cause creation of empty spaces and changes the ordering in the film surface. Due to above-mentioned factors the band gap value decreases with increase in annealing temperature. It is observed that the optical absorption coefficient of the films decreases by increasing the annealing temperature. This effect can be explained by proposing that the annealed film has bigger crystallites resulting in more inter-granular space so the optical density of the film decreases [14].

4. CONCLUSIONS

The present work describes the preparation and characterization of CdS thin films using the CBD technique. The influences of thickness and annealing temperature on structural and optical properties as well as morphology have been reported. All the films presented a mixture of both cubic (sphalerite) and hexagonal (wurtzite) structures, the latter being the most predominant with the hexagonal (100) plane as the preferred orientation. The grain size of the as deposited films was found to increase as the thickness increases from 400 to 1900 Å. With increase in the annealing temperature the grain size was found to increase. Energy band gap value was found to decrease with increase in the thickness as well as with annealing temperature. It is observed that the optical absorption coefficient of the films increases by increasing the thickness, however it decreases by increasing the annealing temperature due to the optical density of the film decreases.

5. ACKNOWLEDGEMENT

6. REFERENCES

[1] Zhibing He, Gaoling Zhao, Wenjian Weng, Piyi Du, Ge Shen, Gaorong Han, Vacuum 79 (2005) 14-18.

[2] K. Senthil, D. Mangalaraj, Sa.K. Narayandass, R. Kesavamoorthy, G.L.N. Reddy, B. Sundaravel, Matter 304 (2001) 175-180.

[3] Jae-Hyeong lee, Dong-Jin Lee, Thin Solid Films 515 (2007) 6055-6059.

[4] Byung-Sik Moon, Jae-Hyeong Lee, Hakkee Jung, Thin Solid Films 511 – 512 (2006) 299 – 303.

[5] J. Hiie, T. Dedova, V. Valdna, K. Muska, Thin Solid Films 511-512 (2006) 443-447.

[6] V. Krishna Kumar, K. Ramamurthi, E. Elangovan, Solid State Communications 132 (2004) 673-677.

[7]   Joo Won Choi, A. Bhupathiraju, M. A. Hasan, John M. Lannon, Crystal Growth 255 (2003) 1-7.

[8] S. Petillon, A. Dinger, M. Grün, M. Hetterich, V. Kazukauskas, C. Klingshirn, J. Liang, B. Weise, V. Wagner and J. Geurts, Crystal Growth 201-202 (1999) 457-460.

[9]   K. Premaratne, S. N. Akuranthilaka, I. M. Dharmadasa and A. P. Samantilleka, Renewable Energy 29 (2003) 549-557.

[10] N. W. Duffy, D. Lane, M. E. Ôzsan, L. M. Peter, K. D. Rogers, R. L. Wang, Thin Solid Film 361-362 (2000) 314-320.

[11] Joel Pantoja Enríquez, Xavier Mathew, Solar Energy Materials and Solar Cells 76 (2003) 313-322.

[12] G. Sasikala, P. Thilakan, C. Subramanian, Solar Energy Materials and Solar Cells 62 (2000) 275.

[13] R. Grecu, E. J. Popovici, M. Ladar, L. Pascu, E. Indreaa, J. Optoelectronics and Advanced Materials 6 (2004) 127 – 132.

[14] H. Metin, R. Esen, J. crystal Growth 258 (2003) 141-148.

[15] E. Çetinörgü, C. Gümüº, R. Esen, Thin Solid Films 515 (2006) 1688-1693.

[16] P.J. Sebastian, Hailin Hu, Advanced Materials for Optical Electronics 4 (1994) 407.

[17] C. Guillén, M. A. Martínez, J. Herrero, Thin Solid Films 335 (1998) 37.

[18] N. G. Dhere, D. L. Waterhouse, K. B. Sundaram, O. Melendez, N. R. Parikh, B. Patnaik, J. Mater. Sci. Mater. Electron 6 (1995) 52.

[20] B.D. Cullity, Elements of X-ray Diffraction, second ed. Addison-Wesley, MA, 1972, p. 102.

[21] G. B. Williamson, R. C. Smallman, Phil. Mag. 1 (1956) 34.

[23] H. P. Kulg, L. E. Alexander, X-ray Diffraction Procedures, John Wiley, New York, 1974, p. 661.

[24] S. Velumani, Xavier Mathew, P. J. Sebastian, Sa. K. Narayandass, D. Mangalaraj, Solar Energy Materials & Solar Cells 76 (2003) 347-358.

[25] S. Prabahar, M. Dhanam, J. Crystal Growth 285 (2005) 41-48.

[26] Jae-Hyeong Lee, Thin Solid Films 515 (2007) 6089-6093.

[27] P.K. Ghosh, S. Jana, U.N. Maity, K.K. Chattopadhyay, Physica E: Low-dimensional Systems and Nanostructures 35 (2006) 178-182.

[28] A. Cortes, H. Gómez, R. E. Marotti, G. Riveros, E. A. Dalchiele, Solar Energy Materials and Solar Cells 82 (2004) 21-34.

[29] P.K. Nair, O. Gomez Daza, A. Arias-Carbajal Readigos, J. Campos, M.T.S. Nair, Semicond. Sci. Technol. 16 (2001) 651.

[30] Jiangrong Xiao, Tianyou Peng, Ke Dai, Ling Zan, Zhenghe Peng, J. Solid State Chemistry 180 (2007) 3188-3195.